



HAL
open science

Modeling of the CO₂ Absorption in a Wetted Wall Column by Piperazine Solutions

Alberto Servia, Nicolas Laloue, Julien Grandjean, Sabine Rode, Christine Roizard

► **To cite this version:**

Alberto Servia, Nicolas Laloue, Julien Grandjean, Sabine Rode, Christine Roizard. Modeling of the CO₂ Absorption in a Wetted Wall Column by Piperazine Solutions. Oil & Gas Science and Technology - Revue d'IFP Energies nouvelles, 2014, 69 (5), pp.885 - 902. 10.2516/ogst/2013136 . hal-01085340

HAL Id: hal-01085340

<https://ifp.hal.science/hal-01085340>

Submitted on 21 Nov 2014

HAL is a multi-disciplinary open access archive for the deposit and dissemination of scientific research documents, whether they are published or not. The documents may come from teaching and research institutions in France or abroad, or from public or private research centers.

L'archive ouverte pluridisciplinaire **HAL**, est destinée au dépôt et à la diffusion de documents scientifiques de niveau recherche, publiés ou non, émanant des établissements d'enseignement et de recherche français ou étrangers, des laboratoires publics ou privés.

Modeling of the CO₂ Absorption in a Wetted Wall Column by Piperazine Solutions

Alberto Servia^{1,2*}, Nicolas Laloue¹, Julien Grandjean¹, Sabine Rode²
and Christine Roizard²

¹ IFP Energies nouvelles, Rond-point de l'échangeur de Solaize, BP 3, 69360 Solaize - France

² LRGP-CNRS Université de Lorraine, 1 rue Grandville, BP 20451, 54001 Nancy Cedex - France

e-mail: alberto.servia@gmail.com

* Corresponding author

Résumé — Modélisation de l'absorption de CO₂ par des solutions de pipérazine dans un film tombant —

Des études théoriques et expérimentales sur l'absorption réactive du CO₂ dans des solutions aqueuses de PZ mettant en œuvre un outil expérimental de type film tombant sont présentées. Un modèle rigoureux d'absorption en deux dimensions, prenant en compte les phénomènes cinétique, thermodynamique et hydrodynamique, a été développé pour simuler l'outil expérimental de film tombant. Les principales originalités du modèle, par rapport aux travaux antérieurs, consistent dans la prise en compte de la variation de la concentration en CO₂ de la phase gaz en fonction de la hauteur du réacteur, ainsi que le calcul de l'équilibre gaz-liquide par une approche thermodynamique cohérente.

Un outil expérimental de type film tombant a été spécialement conçu, pour lequel le coefficient de transfert de masse dans la phase gaz a été estimé. Des mesures d'absorption de CO₂ ont été effectuées sur des solutions aqueuses de PZ, vierges et chargées en CO₂, sur la gamme 298-331 K, et pour des concentrations totales en PZ variant de 0,2 à 1 M. Le modèle de réacteur permet de prédire les flux d'absorption avec une précision remarquable de 3,2 % AAD, que ce soit dans les solutions vierges ou chargées. Le gradient de concentration de CO₂ dans la phase gaz ainsi que la réaction de formation du dicarbamate doivent être pris en compte afin de prédire correctement l'absorption du CO₂ dans les solutions aqueuses de PZ chargées en CO₂.

Abstract — Modeling of the CO₂ Absorption in a Wetted Wall Column by Piperazine Solutions —

Theoretical and experimental investigations on the reactive absorption of CO₂ in aqueous solutions of PZ using a wetted wall column are presented. A rigorous two dimensional absorption model, accounting for kinetics, hydrodynamics and thermodynamics, has been developed for a wetted wall column. Major innovative features of the model, compared to previous work, are the account on the variation of the gas-side CO₂ concentration over the reactor height as well as the computation of the gas-liquid equilibrium by a thermodynamically consistent approach.

A laboratory-scale wetted wall column was conceived and constructed and the gas-side mass-transfer coefficient was estimated. CO₂ absorption experiments were carried out on unloaded and loaded aqueous solutions of PZ over the range of 298-331 K, and for total PZ concentrations varying from 0.2 to 1 M. The reactor model permitted to predict the absorption fluxes in loaded as well as in unloaded solutions with an excellent accuracy, i.e. 3.2% AAD. In loaded solutions, the gas-side CO₂ concentration gradient, as well as the dicarbamate formation reaction has to be taken into account.

NOMENCLATURE**Chemical species**

DEA	DiEthanolAmine
H^+PZCOO^-	Protonated piperazine carbamate
MDEA	N-MethylDiEthanolAmine
MEA	MonoEthanolAmine
PZ	Piperazine
$PZCOO^-$	Piperazine carbamate
$PZ(COO)_2^{2-}$	Piperazine dicarbamate
PZH^+	Protonated piperazine

Others

A	Gas-liquid contact area (m^2)
a	Ratio between the transfer area and the reactor volume (m^{-1})
AAD	Average Absolute Deviation (%)
C^*	Concentration at the gas-liquid interface within the gas phase ($mol.m^{-3}$)
D_h	Hydraulic diameter (m)
D_i	Diffusion coefficient of species “i” ($m^2.s^{-1}$)
E	Enhancement factor adimensional
F	Molar flow ($mol.s^{-1}$)
FEM	Finite Elements Method
G	Gravity acceleration ($m.s^{-2}$)
H	Henry constant ($Pa.m^3.mol^{-1}$)
h	Reactor height (m)
k_G	Gas mass transfer coefficient ($mol.Pa^{-1}.m^{-2}.s^{-1}$)
K_i	Equilibrium constant of reaction i
k_i	Kinetic constant of reaction i ($m^3.mol^{-1}.s^{-1}$)
k_L	Liquid mass transfer coefficient ($m.s^{-1}$)
N	CO_2 flux ($mol.m^{-2}.s^{-1}$)
NRTL	Non Random Two Liquid
pH	$-\log [H^+]$ (adimensional)
pKa	Acid dissociation equilibrium constant adimensional
P	Pressure (Pa)
Q	Volume flow ($m^3.s^{-1}$)
R	Perfect gas law constant ($J.mol^{-1}.K^{-1}$)
r	Radial coordinate (m)
R_i	Reaction rate of chemical reaction i ($mol.m^{-3}.s^{-1}$)
Sh	Sherwood number adimensional
T	Temperature (K)
u	Concentration ($mol.m^{-3}$)

v	Velocity ($m.s^{-1}$)
WWC	Wetted Wall Column
y	Molar fraction
z	Axial coordinate (m)

Greek letters

v_i	Stoichiometric factor associated to species “i” (v_i)
μ	Viscosity (Pa.s)
ρ	Density ($kg.m^{-3}$)
δ	Liquid thickness (m)

Subscripts

app	Apparent
B	Base
G	Gas
L,liq	Liquid
TM	Termolecular
Zw	Zwitterion

Superscripts

eq,*	Equilibrium
in	Inlet
ln	Logarithmic average

INTRODUCTION

Aqueous solutions of alkanolamines are generally used as a solvent for removing acid gases such as CO_2 and H_2S which can be eventually contained in natural gas, hydrogen or flue gas. MonoEthanolAmine (MEA) is the reference alkanolamine for the CO_2 post-combustion capture process while N-MethylDiEthanolAmine (MDEA) is widely used as solvent for natural gas selective deacidification processes. Even if they present high reaction rates with CO_2 , the primary and secondary alkanolamines, such as MEA and DiEthAnolamine (DEA), require a high energy consumption in order to be regenerated. Tertiary amines present lower reaction rates with CO_2 than primary or secondary amines, however the reaction enthalpy is low, which considerably decreases the required energy to regenerate this type of amine.

The addition of a small quantity of a primary or a secondary alkanolamine (activator) into an aqueous solution of a tertiary alkanolamine strongly increases the reaction rate with CO₂ without significantly modifying the energy to provide for the regeneration of the mixture (Chakravarty *et al.*, 1985). Several studies on the kinetics of CO₂ absorption by aqueous blends of alkanolamines can be found in the literature. PZ has revealed itself as being a high-performance activator compared to the conventional alkanolamines such as the MEA or the DEA. Furthermore, BASF commercializes a technology based on the use of a solvent composed by PZ and MDEA (Appl *et al.*, 1982), which illustrates the considerable interest of this cyclic amine. The accurate understanding of the reaction mechanisms between CO₂ and PZ is essential to rigorously investigate the kinetics of CO₂ absorption by MDEA and PZ mixtures.

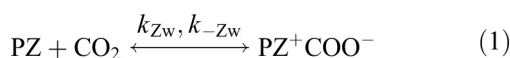
The aim of this work is to study the reactions between the PZ and its derivatives with CO₂. The studies of the kinetics of CO₂ absorption on unloaded and loaded solutions were conducted to evaluate the reaction rates of CO₂ with PZ and PZCOO⁻ respectively. The experimental results were interpreted by a rigorous mathematical model coupling all the phenomena occurring within the reactor. This model also accounts for the CO₂ partial pressure evolution in the gas phase in order to test the hypothesis of considering a constant CO₂ partial pressure given by the logarithmic average between the reactor inlet and outlet.

1 KINETICS

1.1 Reaction Mechanism

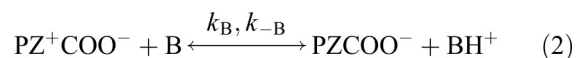
Two mechanisms are proposed in the literature to explain the chemical interactions existing between an amine and CO₂.

The first mechanism, proposed by Caplow (1968) and reintroduced by Danckwerts (1979), is called Zwitterion mechanism. It was widely used to interpret the kinetic data of aqueous solutions of DEA (Rinker *et al.*, 2000; Littell *et al.*, 1992) and of 2-Amino-2-Methyl-1-Propanol (AMP) (Seo and Hong, 2000). This mechanism consists of two steps. Firstly, the amine provides its free electronic pair to form a chemical bond with the carbon atom of the CO₂ molecule to produce an unstable compound called Zwitterion:



The Zwitterion complex is then deprotonated by any base present in the solution, such as PZ, water,

hydroxide ion, etc., to produce a compound called carbamate:



The contribution of each base to the Zwitterion deprotonation depends on its concentration, basicity and steric hindrance.

The CO₂ consumption rate is obtained by assuming the quasi-steady state for the Zwitterion complex and considering that the deprotonation reactions are reversible:

$$r_{\text{CO}_2} = \frac{k_{Zw}[\text{PZ}][\text{CO}_2] \sum_i k_B[\text{B}_i] - k_{-Zw} \sum_i k_{-B}[\text{PZCOO}^-][\text{B}_i\text{H}^+]}{k_{-Zw} + \sum_i k_B[\text{B}_i]} \quad (3)$$

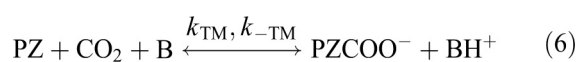
Two limiting cases can be considered for this mechanism. If the deprotonation reaction rate is fast compared to the reverse reaction rate of the Zwitterion formation (k_{-Zw}), the amine partial order is one. The CO₂ rate of consumption is determined using Equation (4), which assumes Zwitterion deprotonation to be irreversible. For instance, this limiting case was verified for MEA, which presents high pKa (9.44 at 298 K, Hamborg and Versteeg, 2009) and no steric hindrance:

$$r_{\text{CO}_2} = k_{Zw}[\text{PZ}][\text{CO}_2] \quad (4)$$

If the deprotonation path is rate limiting and the Zwitterion deprotonation irreversible, the amine partial order varies between 1 and 2, depending on the degree of contribution of each base within the solution. For example, the reaction rate of CO₂ absorption into aqueous DEA solution was determined using Equation (5), involving water and DEA as bases in the Zwitterion deprotonation step (Rinker *et al.*, 1996):

$$r_{\text{CO}_2} = \frac{k_{Zw}[\text{PZ}][\text{CO}_2] \sum_i k_B[\text{B}_i]}{k_{-Zw}} \quad (5)$$

The second mechanism, called the termolecular mechanism, was proposed by Crooks and Donnellan (1989), and reviewed by da Silva and Svendsen (2004). It considers a simultaneous reaction of the amine, CO₂ and a base to produce the carbamate:

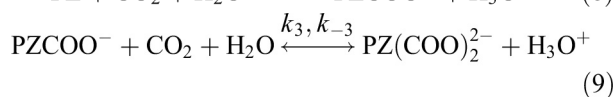
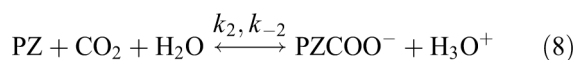


The CO₂ consumption rate is given by the following expression, assuming the reaction irreversibility:

$$r_{\text{CO}_2} = \sum_i k_{\text{TM}}[\text{B}_i][\text{PZ}][\text{CO}_2] - \sum_i k_{-\text{TM}}[\text{B}_i\text{H}^+][\text{PZCOO}^-] \quad (7)$$

If water only contributes to the termolecular mechanism and the reaction is considered as being irreversible, Equation (7) simplifies to Equation (4) with $k_{\text{Zw}} = k_{\text{TM}}[\text{H}_2\text{O}]$. The concentration of water is generally considered as being constant (Bishnoi and Rochelle, 2000; Samanta and Bandyopadhyay, 2007).

The termolecular mechanism is widely used in the literature to explain the chemical reaction existing between CO₂ and PZ (Bishnoi and Rochelle, 2000; Cullinane, 2005; Samanta and Bandyopadhyay, 2007; Dugas, 2009). The authors usually consider one reaction for each amine-function within the PZ molecule:



The CO₂ consumption rate is then given by the following equation, assuming that both reactions are first order in PZ and PZCOO⁻:

$$r_{\text{CO}_2} = k_2[\text{PZ}][\text{CO}_2] - k_{-2}[\text{PZCOO}^-][\text{H}_3\text{O}^+] + k_3[\text{PZCOO}^-][\text{CO}_2] - k_{-3}[\text{PZ}(\text{COO})_2^{2-}][\text{H}_3\text{O}^+] \quad (10)$$

The PZ partial order can be estimated by performing CO₂ absorption experiments into PZ unloaded solutions where the CO₂ mass transfer is not limited by the PZ diffusion towards the gas-liquid interface (pseudo-first order regime). Thus, the CO₂ consumption rate is giving by the following expression:

$$r_{\text{CO}_2} = k_2[\text{PZ}]^{\alpha}[\text{CO}_2] = k_{\text{app}}[\text{CO}_2] \quad (11)$$

The representation of k_{app} as a function of the PZ concentration allows the determination of the PZ partial order.

1.2 Kinetic Constants

Several authors studied the kinetics between CO₂ and PZ (Bishnoi and Rochelle, 2000; Cullinane, 2005; Derks *et al.*, 2006; Samanta and Bandyopadhyay, 2007; Dugas,

2009; Bindwal *et al.*, 2011). The main features of these studies are shown in Table 1.

Bishnoi and Rochelle (2000) performed experiments on unloaded solutions at temperatures ranging from 298 to 333 K and PZ concentrations of 0.2 and 0.6 M. The experimental data obtained in a wetted wall column were used to estimate the second-order kinetic constant of the reaction between PZ and CO₂ and the PZ partial order. A second set of experiments performed on loaded PZ solutions qualitatively shown that the reaction between PZCOO⁻ and CO₂ cannot be neglected at these conditions. The experimental data obtained on unloaded solutions were interpreted by a simple model considering that measurements were carried out in the kinetic regime. They observed that the apparent kinetic constant increased linearly with the PZ concentration, suggesting that this reaction is first order in PZ. Moreover, they determined a second-order kinetic constant (k_2) of 53.7 m³.mol⁻¹.s⁻¹ at 298 K, which is significantly higher than the value obtained by Xu *et al.* (1992) (0.13 m³.mol⁻¹.s⁻¹ at 298 K). Those authors performed experimental tests on loaded solutions, and probably in presence of PZ diffusion limitations towards the gas-liquid interface. The low value of their kinetic constant can be explained by the model developed to interpret the kinetic data which did not account for PZ mass transfer limitations within the liquid phase.

Cullinane (2005) carried out experiments of CO₂ absorption into aqueous PZ solutions by using the same wetted wall column as the one used by Bishnoi and Rochelle (2000). The author proposed a reaction mechanism based on Brönsted theory, which states that the kinetic constant associated to the reactions generating PZCOO⁻ and PZ(COO⁻)₂ (PZ (or PZCOO⁻), CO₂ and a base: OH⁻, H₂O, PZ, CO₃²⁻ and PZCOO⁻) depends on the pKa of the considered base. The contribution of the hydroxyl ions as a base for catalyzing the chemical reaction between PZCOO⁻ and CO₂ was neglected since OH⁻ and PZCOO⁻ does not coexist within the liquid solution. Three other chemical reactions were also considered to account for the bicarbonate formation in the reaction mechanism (CO₂, H₂O and a base: H₂O, PZ and PZCOO⁻). The impact of the addition of a neutral salt into the amine solution on the global CO₂ absorption kinetics was also investigated. The reaction rate was found to increase with the ionic strength. The same evolution was observed in the case of the CO₂ absorption into aqueous solutions of PZ and K₂CO₃. Indeed, the presence of K₂CO₃ in the solution increases the bases concentration within the liquid phase (OH⁻ and CO₃²⁻) and therefore enhances the reaction rate. Moreover, Cullinane (2005), estimated a

TABLE 1
Literature review on the kinetics study of CO₂ absorption by aqueous PZ solutions

Reference	Experimental device	Loading mol _{CO₂} /mol _{PZ}	[PZ] (M)	T (K)	k_2 (m ³ .mol ⁻¹ .s ⁻¹)	k_3 (m ³ .mol ⁻¹ .s ⁻¹)	Kinetic modeling	Mass transfer	Comments
Xu <i>et al.</i> , 1992	Disk column	(0.2393-2.138) × 10 ³ mol.m ⁻³	0.041-0.21 (mixtures with MDEA)	303-343	0.13 at 298 K	-	Pseudo-first order	Film theory and no k_G (Pure CO ₂)	Loaded solutions
Bishnoi and Rochelle, 2000	Wetted wall column	0-0.67	0.2 and 0.6	298-333	$53.7 \exp\left(-\frac{36000}{R}\left[\frac{1}{T} - \frac{1}{298}\right]\right)$	-	Pseudo-first order	Film theory	No interpretation of the data taken on loaded solutions
Bishnoi and Rochelle, 2002	Wetted wall column	0.0011-0.625	0.6 (mixture with MDEA 4 M)	295-343	$53.7 \exp\left(-\frac{36000}{R}\left[\frac{1}{T} - \frac{1}{298}\right]\right)$	$47.0 \exp\left(-\frac{36000}{R}\left[\frac{1}{T} - \frac{1}{298}\right]\right)$	Liquid discretization with constant CO ₂ partial pressure	Eddy theory (constant P_{CO_2} within the gas)	Complex kinetics considering synergy between both amines
Cullinane, 2005	Wetted wall column	0-0.019	0.45-1.20 m	298 and 333	-	-	Liquid discretization with constant CO ₂ partial pressure	Eddy theory (constant P_{CO_2} within the gas)	Second order on PZ for [PZ] > 0.5 M and study of impact from neutral salts and K ₂ CO ₃ addition
Derks <i>et al.</i> , 2006	Stirred cell	0	0.6-1.5	293-313	70.0 at 298 K	-	DeCoursey (1974) and Hogendoorn <i>et al.</i> (1997)	Film theory and no k_G (pure CO ₂)	Kinetics of reaction between PZH ⁺ and CO ₂ quantified
Samanta and Bandyopadhyay (2007)	Wetted wall column	0	0.2-0.8	298-313	58.0 at 298 K	59.5 at 298 K	Complex model with constant CO ₂ partial pressure	Penetration theory (constant P_{CO_2} within the gas)	Kinetics of the reaction between PZCOO ⁻ and CO ₂ quantified
Dugas, 2009	Wetted wall column	0.222-0.412	2-12 m m = molality	313-373	-	-	Pseudo- m,n^{th} order corrected with species activity coefficients	Double film theory	Second order on PZ
Bindwal <i>et al.</i> , 2011	Stirred cell	0	0.025-0.1	303	25.8 at 303 K	-	Pseudo-first order	Film theory and no impact from k_G verified	Unloaded solutions

partial order of 2 for the PZ for an amine concentration higher than 0.5 M. This result does not agree with the work of Bishnoi and Rochelle (2000) that determined a partial order of 1 for the PZ, based on measurements on 0.2 and 0.6 M PZ solutions.

Derks *et al.* (2006) determined a value for k_2 of $70.0 \text{ m}^3 \cdot \text{mol}^{-1} \cdot \text{s}^{-1}$ at 298 K through experiments carried out in a stirred cell. They also quantified the kinetics of the reaction between the PZH^+ and CO_2 by performing a new set of experimental CO_2 absorption measurements on partially protonated PZ. The kinetic constant associated to this reaction was $0.280 \pm 0.100 \text{ m}^3 \cdot \text{mol}^{-1} \cdot \text{s}^{-1}$ at 298 K, which is in agreement with the Bronsted theory.

Samanta and Bandyopadhyay (2007) developed a mathematical model accounting for mass transfer, kinetics and equilibrium phenomena to estimate the kinetics of the reactions between PZ and piperazine carbamate (PZCOO^-) and CO_2 . Their experimental data were performed in a wetted wall column. The kinetic constants obtained were in good agreement with those determined by Bishnoi and Rochelle (2000, 2002). The consistency between these values cannot be justified through the use of the same device since kinetics determination strongly depends on the mathematical model used to interpret the experimental data.

Dugas (2009) performed experiments in the same wetted wall column as the one used by Bishnoi (2000) and Cullinane (2005). This work considered an activity-based reaction mechanism based on the Brønsted theory. Both PZ and PZCOO^- were involved as bases for catalyzing the chemical reactions between PZ and CO_2 , and between PZCOO^- and CO_2 , implicitly assuming a partial order of 2 for PZ, in agreement with Cullinane (2005).

Finally, Bindwal *et al.* (2011) observed that the second-order kinetic constant increases with the PZ concentration. They determined a value of $25.8 \text{ m}^3 \cdot \text{mol}^{-1} \cdot \text{s}^{-1}$ at 303 K, which is considerably lower than the one obtained by Bishnoi and Rochelle (2000).

Many discrepancies exist concerning the kinetics of CO_2 absorption by aqueous PZ solutions. The results depend on the type of model involved to interpret the experimental measurements as well as on the experimental device. The easiest way to determine kinetics is through the pseudo-first order assumption, allowing the kinetics to be analytically determined. Nevertheless, the use of this simple mass transfer model is only suitable for a specific and narrow range of experimental conditions. Its use can lead to large errors if mass transfer limitations within the liquid phase are involved (Xu *et al.*, 1992). The kinetics of the CO_2 absorption in a wide range of operating conditions can only be determined by accurately describing all phenomena occurring within

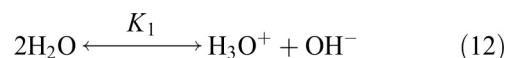
the reactor. Besides, even if the gas mass transfer resistance represents a non negligible part of the total mass transfer resistance, all studies from the literature consider a constant CO_2 partial pressure to describe the CO_2 mass transfer, which can lead to errors in the CO_2 flux determination.

2 MODELING SECTION

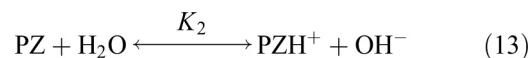
2.1 Chemical Reactions

Two types of chemical reactions were considered in the reactor model: equilibrium reactions and reactions limited by kinetics. The chemical reactions involving a single transfer of proton were considered instantaneous (Cullinane, 2005; Samanta and Bandyopadhyay, 2007). They were described by their equilibrium constant:

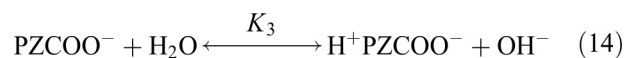
Water dissociation



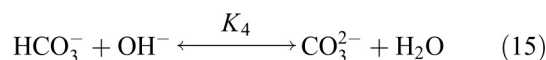
PZ protonation



PZCOO⁻ protonation



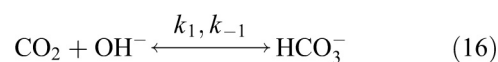
Carbonate formation



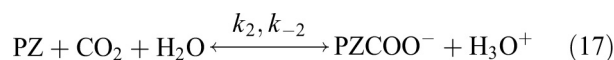
The carbonic acid equilibrium reaction was not considered in the system due to the high pH of the aqueous alkanolamine solutions. The equilibrium constants associated to each reaction were given by the thermodynamic model which is described later in this paper.

Beyond the equilibrated reactions, the chemical reactions involving CO_2 were considered to be kinetically controlled:

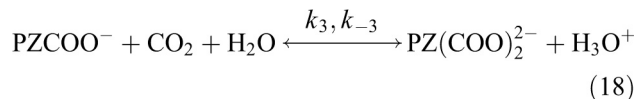
Bicarbonate formation



Piperazine carbamate formation



Piperazine dicarbamate formation



The CO₂ hydrolysis was neglected as its reaction rate is low compared to the other chemical reactions considered in the kinetic network (Bishnoi and Rochelle, 2000; Samanta and Bandyopadhyay, 2007). The kinetic constant for the bicarbonate formation was obtained from the paper of Pinsent *et al.* (1956) while the kinetic constants of the reactions between piperazine, and piperazine carbamate with CO₂ were taken from the papers of Bishnoi and Rochelle (2000, 2002), respectively. The kinetic constant expression associated to the chemical reaction between the PZCOO⁻ and CO₂ was given by the following equation.

$$k_2 = 47.0 \exp\left(-\frac{36000}{R} \left[\frac{1}{T} - \frac{1}{298}\right]\right) \quad (19)$$

All reactions were considered to be reversible in this work.

2.2 Thermodynamics

The thermodynamic model used in this work was provided by ASPEN Plus. It allowed to compute the concentration of each species within the liquid phase as well as the CO₂ equilibrium vapour pressure. The activity coefficients of all the species within the liquid phase were taken into account through the electrolyte NRTL approach while the Redlich-Kwong-Soave state equation was used to determine the gas phase deviation from the ideal state (Bishnoi and Rochelle, 2000; Cullinane, 2005). The thermodynamic model was validated by comparison with vapour-liquid equilibrium data from literature (Bishnoi and Rochelle, 2000; Hilliard, 2005). Figure 1 is plotted at a fixed temperature of 313 K whereas Figure 2 represents the equilibrium at 2 different temperatures (333 K and 343 K). The equilibrium pressure obviously varies with temperature as well as with loading (Fig. 3). Consequently, it is the temperature that makes the difference, not the PZ overall concentration.

The $P_{\text{CO}_2}^*$ also increases with temperature and remains almost independent of PZ concentration (Fig. 1, 2). The AAD between experimental and modelled CO₂ vapour pressure was 19%.

The solubility was calculated by the ratio between the CO₂ equilibrium vapour pressure and the CO₂ liquid concentration provided by a flash calculation in ASPEN Plus (Fig. 3). The calculated values were in good agreement with the solubilities determined through the N₂O

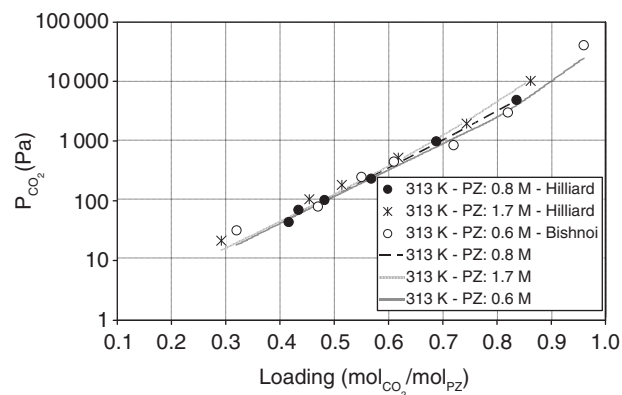


Figure 1

Vapour-liquid equilibrium CO₂ partial pressure as a function of the solution loading at 313 K; symbols: literature data; lines: model calculations.

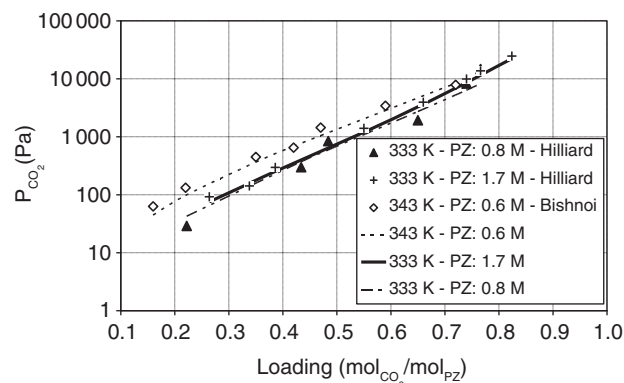


Figure 2

Vapour-liquid equilibrium CO₂ partial pressure as a function of the solution loading at 333 and 343 K; symbols: literature data; lines: model calculations.

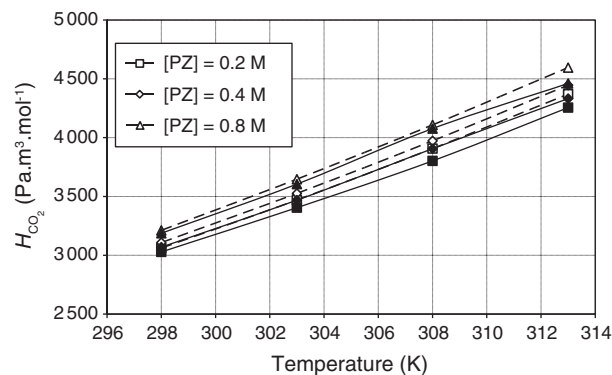


Figure 3

Solubility of CO₂ as a function of temperature at different PZ concentrations. Empty symbols: computed values; filled symbols: N₂O analogy.

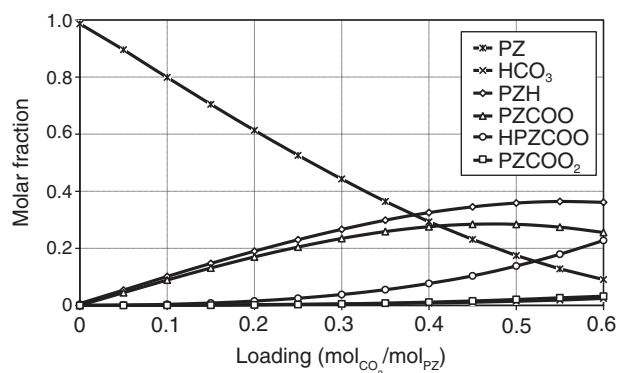


Figure 4

Speciation estimated by the ASPEN Plus thermodynamic model for a solution of 1 M of PZ at 298 K.

analogy semi-empirical approach by Samanta *et al.* (2007), with an AAD of 1.8%. Consequently, the use of the N₂O analogy to determine CO₂ solubility would be possible in this case, since both the solubilities given by the thermodynamic model and by N₂O analogy are similar in the range of tested temperatures. However, the difference between values computed using ASPEN Plus and N₂O analogy increases with temperature which shows that the use of the N₂O analogy at higher temperatures leads to more discrepancy.

The thermodynamic model described in this section was used to determine the solution loading corresponding to the highest concentration of PZCOO⁻, in order to evaluate its reaction with CO₂. The thermodynamic model predicted a maximum of PZCOO⁻ concentration at a loading of approximately 0.5 at 298 K, which is in agreement with Bishnoi and Rochelle (2000) (Fig. 4). The maximum of PZCOO⁻ concentration was comparable at 333 K (data not shown).

2.3 Hydrodynamics

The liquid phase velocity profile was determined using the Navier-Stokes equation for an incompressible fluid associated with specific boundary conditions. The velocity profile was considered to be fully developed at the reactor inlet. Hydrodynamic calculations performed in Fluent, not shown here, supported the validity of this assumption:

$$0 = \mu_{\text{liq}} \left[\frac{\partial^2 v_L(r)}{\partial r^2} + \frac{1}{r} \frac{\partial v_L(r)}{\partial r} \right] - \rho_{\text{liq}} g \quad (20)$$

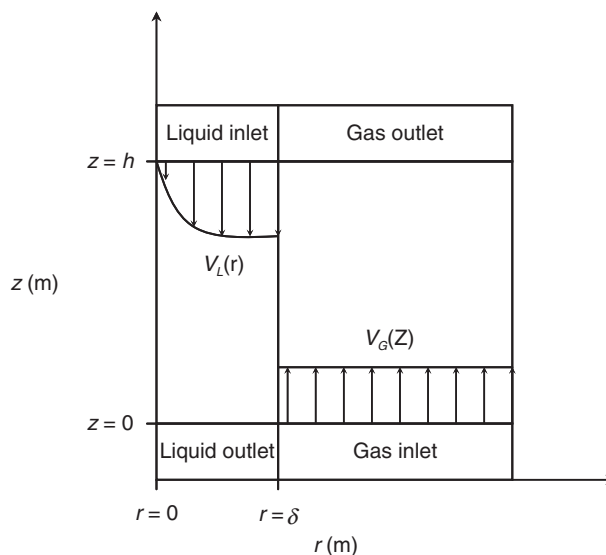


Figure 5

Schematic representation of the reactor geometry.

$$v_L(r=0) = 0 \quad (21)$$

$$\frac{\partial v_L(r=\delta)}{\partial r} = 0 \quad (22)$$

where δ represents the liquid film thickness. The radial (r) and axial (z) coordinates are illustrated in Figure 5.

The gas phase velocity was obtained by performing a mass balance on the nitrogen (N₂). A plug-flow model was used in order to describe the gas phase flow:

$$v_G(z) = \frac{Q_G^{\text{in}} (1 - y_{\text{CO}_2}^{\text{in}}) P}{A (P - C_{\text{CO}_2}^G RT)} \quad (23)$$

where Q_G^{in} and $y_{\text{CO}_2}^{\text{in}}$ represent the total gas flow and the CO₂ molar fraction at the reactor inlet, respectively. The total pressure P was supposed constant within the reactor.

2.4 Reactor Model

A 2D stationary model was developed using COMSOL software to predict the absorption flux of CO₂ into aqueous solutions of PZ within a wetted wall column. This model couples hydrodynamics, mass transfer, chemical reactions and gas-liquid equilibrium. One of the model originalities is the description of the CO₂ partial pressure variation within the gas phase, instead of considering a constant CO₂ partial pressure given by the logarithmic average between the reactor inlet and outlet.

The concentration profile of each chemical species within the liquid phase, $u_i(r,z)$, was obtained by the simultaneous resolution of the mass balance for each compound, the electroneutrality condition and the equilibrium constants associated to the instantaneous-considered proton-transfer reactions.

The species concentrations were renamed as follows in order to simplify the presentation of the algebraic-differential equation system:

CO₂ - u_1 , PZ - u_2 , H₃O⁺ - u_3 , OH⁻ - u_4 , PZH⁺ - u_5 , PZCOO⁻ - u_6 , H⁺PZCOO⁻ - u_7 , PZ(COO)₂²⁻ - u_8 , HCO₃⁻ - u_9 and CO₃²⁻ - u_{10} .

– CO₂ mass balance:

$$0 = D_{u_1} \left(\frac{\partial^2 u_1}{\partial r^2} + \frac{1}{r} \frac{\partial u_1}{\partial r} + \frac{\partial^2 u_1}{\partial z^2} \right) - v_L(r) \frac{\partial u_1}{\partial z} - (R_1 + R_2 + R_3) \quad (24)$$

– global PZ mass balance:

$$0 = D_{u_2} \left(\frac{\partial^2 u_2}{\partial r^2} + \frac{1}{r} \frac{\partial u_2}{\partial r} + \frac{\partial^2 u_2}{\partial z^2} \right) + D_{u_5} \left(\frac{\partial^2 u_5}{\partial r^2} + \frac{1}{r} \frac{\partial u_5}{\partial r} + \frac{\partial^2 u_5}{\partial z^2} \right) + D_{u_6} \left(\frac{\partial^2 u_6}{\partial r^2} + \frac{1}{r} \frac{\partial u_6}{\partial r} + \frac{\partial^2 u_6}{\partial z^2} \right) + D_{u_7} \left(\frac{\partial^2 u_7}{\partial r^2} + \frac{1}{r} \frac{\partial u_7}{\partial r} + \frac{\partial^2 u_7}{\partial z^2} \right) + D_{u_8} \left(\frac{\partial^2 u_8}{\partial r^2} + \frac{1}{r} \frac{\partial u_8}{\partial r} + \frac{\partial^2 u_8}{\partial z^2} \right) - v_L(r) \left[\frac{\partial u_2}{\partial z} + \frac{\partial u_5}{\partial z} + \frac{\partial u_6}{\partial z} + \frac{\partial u_7}{\partial z} + \frac{\partial u_8}{\partial z} \right] \quad (25)$$

– global PZCOO⁻ mass balance:

$$0 = D_{u_6} \left(\frac{\partial^2 u_6}{\partial r^2} + \frac{1}{r} \frac{\partial u_6}{\partial r} + \frac{\partial^2 u_6}{\partial z^2} \right) + D_{u_7} \left(\frac{\partial^2 u_7}{\partial r^2} + \frac{1}{r} \frac{\partial u_7}{\partial r} + \frac{\partial^2 u_7}{\partial z^2} \right) + v_L(r) \left[\frac{\partial u_6}{\partial z} + \frac{\partial u_7}{\partial z} \right] + R_2 - R_3 \quad (26)$$

– global PZ(COO)₂²⁻ mass balance:

$$0 = D_{u_8} \left(\frac{\partial^2 u_8}{\partial r^2} + \frac{1}{r} \frac{\partial u_8}{\partial r} + \frac{\partial^2 u_8}{\partial z^2} \right) + v_L(r) \frac{\partial u_8}{\partial z} + R_3 \quad (27)$$

– global carbon mass balance:

$$0 = D_{u_1} \left(\frac{\partial^2 u_1}{\partial r^2} + \frac{1}{r} \frac{\partial u_1}{\partial r} + \frac{\partial^2 u_1}{\partial z^2} \right) + D_{u_6} \left(\frac{\partial^2 u_6}{\partial r^2} + \frac{1}{r} \frac{\partial u_6}{\partial r} + \frac{\partial^2 u_6}{\partial z^2} \right) + D_{u_7} \left(\frac{\partial^2 u_7}{\partial r^2} + \frac{1}{r} \frac{\partial u_7}{\partial r} + \frac{\partial^2 u_7}{\partial z^2} \right) + 2 \times D_{u_8} \left(\frac{\partial^2 u_8}{\partial r^2} + \frac{1}{r} \frac{\partial u_8}{\partial r} + \frac{\partial^2 u_8}{\partial z^2} \right) + D_{u_9} \left(\frac{\partial^2 u_9}{\partial r^2} + \frac{1}{r} \frac{\partial u_9}{\partial r} + \frac{\partial^2 u_9}{\partial z^2} \right) + D_{u_{10}} \left(\frac{\partial^2 u_{10}}{\partial r^2} + \frac{1}{r} \frac{\partial u_{10}}{\partial r} + \frac{\partial^2 u_{10}}{\partial z^2} \right) - v_L(r) \left[\frac{\partial u_1}{\partial z} + \frac{\partial u_6}{\partial z} + \frac{\partial u_7}{\partial z} + 2 \times \frac{\partial u_8}{\partial z} + \frac{\partial u_9}{\partial z} + \frac{\partial u_{10}}{\partial z} \right] \quad (28)$$



Figure 6

Gas phase distributor.

– electroneutrality balance:

$$0 = D_{u_3} \left(\frac{\partial^2 u_3}{\partial r^2} + \frac{1}{r} \frac{\partial u_3}{\partial r} + \frac{\partial^2 u_3}{\partial z^2} \right) + D_{u_4} \left(\frac{\partial^2 u_4}{\partial r^2} + \frac{1}{r} \frac{\partial u_4}{\partial r} + \frac{\partial^2 u_4}{\partial z^2} \right) - D_{u_5} \left(\frac{\partial^2 u_5}{\partial r^2} + \frac{1}{r} \frac{\partial u_5}{\partial r} + \frac{\partial^2 u_5}{\partial z^2} \right) - 2 \times D_{u_6} \left(\frac{\partial^2 u_6}{\partial r^2} + \frac{1}{r} \frac{\partial u_6}{\partial r} + \frac{\partial^2 u_6}{\partial z^2} \right) - 2 \times D_{u_7} \left(\frac{\partial^2 u_7}{\partial r^2} + \frac{1}{r} \frac{\partial u_7}{\partial r} + \frac{\partial^2 u_7}{\partial z^2} \right) - 2 \times D_{u_8} \left(\frac{\partial^2 u_8}{\partial r^2} + \frac{1}{r} \frac{\partial u_8}{\partial r} + \frac{\partial^2 u_8}{\partial z^2} \right) - v_L(r) \left[\frac{\partial u_3}{\partial z} - \frac{\partial u_4}{\partial z} + \frac{\partial u_5}{\partial z} - \frac{\partial u_6}{\partial z} - 2 \times \frac{\partial u_7}{\partial z} - \frac{\partial u_8}{\partial z} - 2 \times \frac{\partial u_{10}}{\partial z} \right] \quad (29)$$

– K_1 : 2H₂O ↔ H₃O⁺ + OH⁻

$$K_1 = u_3 \times u_4 \quad (30)$$

– K_2 : PZ + H₂O ↔ PZH⁺ + OH⁻

$$K_2 = \frac{u_5 \times u_4}{u_2} \quad (31)$$

– K_3 : PZCOO⁻ + H₂O ↔ H⁺PZCOO⁻ + OH⁻

$$K_3 = \frac{u_7 \times u_4}{u_6} \quad (32)$$

– K_4 : CO₃²⁻ + H₂O ↔ HCO₃⁻ + OH⁻

$$K_4 = \frac{u_9 \times u_4}{u_{10}} \quad (33)$$

The kinetics expressions used in the mass balance equations are given as follows:

$$R_1 = k_1[\text{CO}_2][\text{OH}^-] - \frac{k_1}{K_1}[\text{HCO}_3^-] \quad (34)$$

$$R_2 = k_2[\text{CO}_2][\text{PZ}] - \frac{k_2}{K_2}[\text{PZCOO}^-][\text{H}_3\text{O}^+] \quad (35)$$

$$R_3 = k_3[\text{CO}_2][\text{PZCOO}^-] - \frac{k_3}{K_3}[\text{PZ}(\text{COO})_2^{2-}][\text{H}_3\text{O}^+] \quad (36)$$

The partial differential-algebraic system composed by 10 equations was solved using the finite element method (FEM) in COMSOL Multiphysics. It led to the determination of the concentration profiles $C_i(r,z)$ in the liquid phase. Following boundary conditions are applied:

$$u_i(r, z = h) = u_i^{\text{eq}} \quad (37)$$

$$\frac{\partial u_i(r, z = 0)}{\partial z} = 0 \quad (38)$$

$$\frac{\partial u_i(r = 0, z)}{\partial r} = 0 \quad (39)$$

$$\frac{\partial u_i(r = \delta, z)}{\partial r} = 0 \quad i \neq \text{CO}_2 \quad (40)$$

$$D_1 \frac{\partial u_1(r = \delta, z)}{\partial r} = k_G(P_{\text{CO}_2} - Hu_1(r = \delta, z)) \quad (41)$$

where h represents the reactor height, H the Henry constant and P_{CO_2} the CO_2 partial pressure in the gas phase.

The concentration of each species at equilibrium conditions were provided by the thermodynamic model described in Section 2.3. The estimated concentrations were used to determine the apparent equilibrium constants of the chemical reactions. The CO_2 Henry constant was determined by the ratio between P_{CO_2} and the molecular CO_2 concentration at equilibrium conditions. This is original, as it is generally estimated in literature using a N_2O analogy.

The use of the same Henry constant for the determination of both interface and liquid compositions, allows the consistency between the global mass transfer driving force defined by the CO_2 partial pressures in the gas and liquid phases and the predicted liquid CO_2 driving force determined at the interface. This is not satisfied when two different solubility values are used.

As CO_2 is absorbed, P_{CO_2} presents a decreasing profile within the reactor. Consequently, the model takes into account the evolution of the CO_2 partial pressure in the gas phase through a one-dimensional plug-flow

model (Eq. 42). The flow can be considered countercurrent since the ratio $h/D_h \gg 1$ and the gas velocity is substantially higher than the liquid velocity. Moreover, the gas distribution has been improved by multiple injection points and the addition of a gas distributor (Fig. 8). Besides, simulations performed with FLUENT software have shown that the flow is essentially countercurrent:

$$0 = \frac{\partial (v_G C_{\text{CO}_2}^G)}{\partial z} + k_G a (P_{\text{CO}_2} - Hu_1(r = \delta, z)) \quad (42)$$

The average CO_2 flux across the gas-liquid interface was determined using the following expression:

$$N_{\text{CO}_2} = \frac{\int_{z=h}^{z=0} D_{u_1} \frac{\partial u_1(r=\delta, z)}{\partial r} dz}{h} \quad (43)$$

2.5 Physicochemical Properties

Properties such as the CO_2 and PZ diffusion coefficients must be known in order to determine the concentration profiles of the different species. The CO_2 diffusion coefficient in water can be obtained through the following correlation (Bishnoi and Rochelle, 2000):

$$D_{\text{CO}_2} = 0.02397 \exp\left(\frac{-2122.2}{T(\text{K})}\right) \quad (44)$$

The PZ concentration and the solution loading are not considered in this correlation.

The diffusion coefficients of PZ and of the ionic species were estimated by multiplying the CO_2 diffusion coefficient by 0.7. This is in agreement with the work of Bishnoi (2000), that has shown that the ratio between the diffusion coefficients of the ionic species and CO_2 is comprised between 0.7 and 0.8. Anyway, the ratio considered has not a major influence on the simulation results as the selected experimental operating conditions allow to avoid a significant impact of diffusion limitations of PZ and ionic species in the liquid phase on the CO_2 transfer (Fig. 7).

2.6 Comparison Between Gas Mass Transfer Models

A plug flow reactor model was used in this work to describe the P_{CO_2} evolution within the gas phase. This one-dimensional model was compared to the traditional approach of considering a constant CO_2 partial pressure

given by the logarithmic average between the reactor gas inlet and outlet, given by:

$$P_{\text{CO}_2}^{\text{ln}} = \frac{P_{\text{CO}_2}^{\text{inlet}} - P_{\text{CO}_2}^{\text{outlet}}}{\ln \frac{P_{\text{CO}_2}^{\text{inlet}}}{P_{\text{CO}_2}^{\text{outlet}}} } \quad (45)$$

The boundary condition at the gas-liquid interface remaining the same (Eq. 41), the only difference between both models is the estimation of P_{CO_2} .

Simulations at two different operating conditions were carried out in order to illustrate the difference between both approaches. The chosen operating conditions and the estimated fluxes obtained are shown in Table 2.

The difference between simulated fluxes given by the two approaches is negligible in unloaded solutions whereas it is of about 16% for a loading of 0.4. Appendix A shows that the results given by both approaches are identical for unloaded solution when

the CO₂ partial pressure at the gas-liquid interface does not change with the reactor height.

2.7 Choice of the CO₂ Partial Pressure

The CO₂ mass transfer in a wetted wall column is a function of the gas mass transfer, the liquid mass transfer, reactions rates, CO₂ solubility, etc. In order to maximize the sensitivity of the model calculations to the values of the kinetic constants, the experimental tests must be carried out in conditions minimizing the resistances due to the PZ mass transfer within the liquid towards the gas-liquid interface. The reactor model was used to identify these conditions.

Figure 7 illustrates the simulated PZ concentration at the gas-liquid interface at $z = 0$ as a function of the CO₂ molar fraction at the gas inlet. Unloaded solutions were considered. Figure 7 shows that PZ is almost depleted at the gas-liquid interface for the high CO₂ partial pressure. For the low CO₂ partial pressure, the PZ depletion at the gas-liquid interface is low, which means that the CO₂ mass transfer is mostly limited by the chemical reactions carried out within the solution. The kinetics of CO₂ absorption can be accurately determined in these conditions.

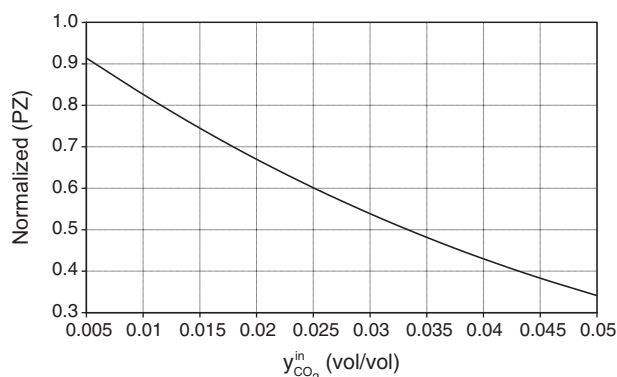


Figure 7

Simulated normalized PZ concentration at the reactor outlet at the gas-liquid interface at 298 K and 0.2 M of PZ (unloaded solution) as a function of CO₂ molar fraction in the gas phase at the gas inlet ($z = 0$).

3 EXPERIMENTAL DEVICE

The experiments were conducted in a wetted wall column at temperatures ranging from 298 to 333 K on unloaded and loaded aqueous solutions of PZ. The solution loading was up to 0.4 mol_{CO₂}/mol_{amine} while the PZ concentrations range was comprised between 0.2-1 M.

The wetted wall column is a suitable equipment to obtain kinetic data of gas-liquid systems presenting high reaction rates due, to the high values of liquid mass transfer coefficients (k_L) associated to this device. The wetted wall column consists of a stainless steel cylinder with a surface area of 36.02 cm² (Fig. 8). The height and external diameter of the reactor are 9.1 and 1.26 cm, respectively. Within the reactor, the gas phase

TABLE 2

CO₂ fluxes simulated considering the local CO₂ pressure in the gas phase (model) or a Traditional Approach (TA) *i.e.* the logarithmic average of the CO₂ partial pressure

Temperature (K)	[PZ] (M)	Loading (mol _{CO₂} /mol _{PZ})	Flux model ($\times 10^3$) (mol.m ⁻² s ⁻¹)	Flux TA ($\times 10^3$) (mol.m ⁻² s ⁻¹)
328	1	0.4	1.12	0.94
319	1	0	1.79	1.78

TA – Traditional Approach.

$Q_L = 16$ L/h, $Q_G = 150$ NL/h, $P = 1.5$ bar, $y_{\text{CO}_2}^{\text{in}} = 7000$ ppm.

flows counter-currently with the liquid that overflows from the inside of a cylinder to form a thin liquid film.

The gas phase, composed of CO₂ and nitrogen (N₂), is water-saturated before being in contact with the liquid in the reactor to prevent from water mass transfer in the reaction zone. The gas phase enters the reactor by 4 injection points. A gas distributor (Fig. 6) is located at the reactor inlet, just above the 4 injection points, in order to achieve an efficient gas distribution in the reaction zone. Downstream the reactor, the water contained in the gas is condensed within two consecutive condensers. The water-free gas is finally sent to an infra-red spectrometer that measures in-line the CO₂ gas concentration. The experimental flux is determined by the variation of the CO₂ gas concentration at both the inlet and the outlet of the reactor.

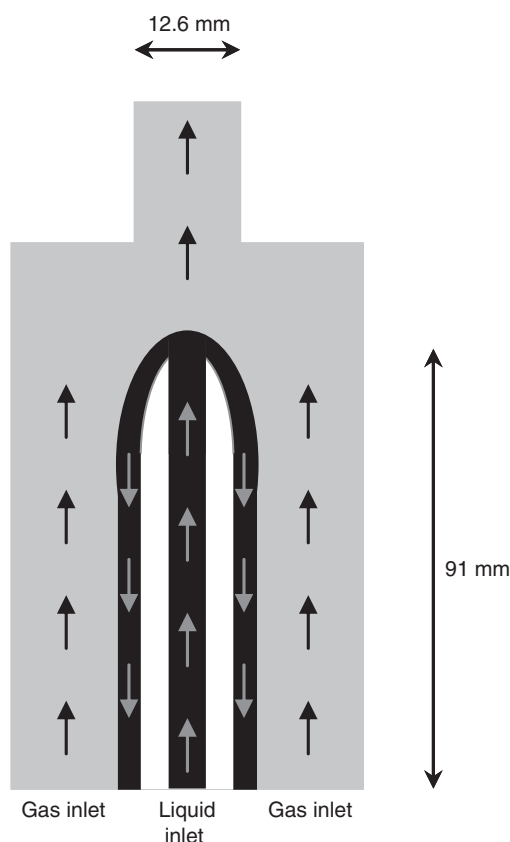


Figure 8
Wetted Wall Column (WWC) scheme.

4 RESULTS AND DISCUSSION

4.1 Gas Phase Mass Transfer Coefficient

The gas-side mass transfer resistance can generally not be neglected in reactive absorption. Hence the correct estimation of the gas-side mass transfer coefficient is crucial to accurately model the overall process. The gas phase mass transfer coefficient was measured by performing experiments of CO₂ absorption in aqueous solutions of MEA. The kinetics and the thermodynamics of MEA are well established in the literature, which justifies the choice of this system to determine the gas side mass transfer coefficient k_G . Besides, this system was used by Pacheco (1998), to estimate mass transfer resistance in gas phase in a similar device. The correlation obtained by Pacheco (1998) was later confirmed by the work of Bishnoi (2000), who performed measurements on a system presenting an instantaneous chemical reaction (SO₂/NaOH). All experiments were performed at a gas flow of 150 L/h and at a constant temperature of 333 K. The absorption tests were carried out on unloaded MEA solutions with overall concentrations ranging from 0.5 to 2 M. The total pressure was set to 1.5 bar. Experiments conducted at different solvent concentrations led to the simultaneous determination of the gas-liquid contact area, A , and of the volumetric gas-side mass transfer coefficient, k_G . A gas-liquid contact area of 38 cm² was estimated with an experimental error of approximately 10%. This value is in agreement with the geometric area of 36.02 cm². The experimentally determined volumetric mass transfer coefficient k_G , reported in Table 3, was consistent with the solution given by Graetz in a developed mass transfer boundary layer ($Sh_{lim} = 3.66$), however the accuracy was not very high. More details are given in Appendix B. k_G values at 298 and at 319 K were estimated assuming a constant Sherwood number. The estimation of k_G values at another temperature only depends on the CO₂ diffusion coefficient:

$$Sh = \frac{k_G D_h}{D_{CO_2}} = \text{constant} \Rightarrow \frac{k_G(T)}{k_G(T')} = \frac{D_{CO_2}(T)}{D_{CO_2}(T')} \quad (46)$$

The CO₂ diffusion coefficient in N₂ was estimated using the kinetic theory of gases (Poling *et al.*, 2000).

TABLE 3

Estimation of the gas-liquid volumetric mass transfer coefficient at different temperatures

Temperature (K)	298 (Calculated)	319 (Calculated)	333 (Experimental)
k_G (mol.Pa ⁻¹ .m ⁻² .s ⁻¹)	6.6×10^{-6}	7.2×10^{-6}	$(7.8 \pm 3.9) \times 10^{-6}$

Resulting estimations of the gas-liquid volumetric mass transfer coefficient are reported in Table 3.

4.2 CO₂ Absorption in Aqueous PZ Solutions

Two set of experimental tests were carried out in order to characterize the kinetics of the reactions between the PZ and the PZCOO⁻ with CO₂. All experimental tests were carried out at constant pressure (1.5 bar) and at a fixed dry CO₂ molar fraction in the gas phase at the reactor inlet (about 7 000 ppm). The liquid and gas flow rates were set to 16 and 150 L/h, respectively. The operating temperature varied between 293 and 331 K.

A large experimental error was expected from the experiments conducted at 298 K since no temperature regulation could be applied. These measurements were performed at ambient temperature, which was comprised between 293 and 298 K.

An average relative gas-side mass transfer-resistance was estimated considering Equation (47):

$$\underbrace{\frac{H}{Ek_L}}_{\text{Liquid phase}} + \underbrace{\frac{1}{k_G}}_{\text{Gas phase}} = \frac{\Delta P_{\text{CO}_2}^{\text{ln}}}{N_{\text{CO}_2}} \quad (47)$$

The average relative gas-side mass transfer-resistance was comprised between 18 and 35% as reported in Tables 4 and 5. The high value clearly demonstrates the requirement of a correct estimation of the gas-side mass transfer coefficient for data interpretation.

4.2.1 Unloaded Solutions

CO₂ absorption experiments were conducted at temperatures between 298 and 331 K on unloaded PZ solutions ranging from 0.2 to 1 M. Experimental results and corresponding simulations are reported in Table 4. The simulations were performed considering the experimental temperature and input CO₂ molar fraction.

Model predictions were in good agreement with experimental data, except for the experiment at 297 K in a 1 M PZ solution which might be erroneous. The AAD between the experimental and model data was 3.7%.

The variation of the absorption flux with the total PZ concentration is shown in Figure 9 for three different temperatures. Again, measurements and simulations are shown. The simulations depicted in Figure 9 were performed at the average temperature and CO₂ inlet molar fraction of the measurement series.

The absorption flux increases with the total PZ concentration, as expected, due to the increase of the

reaction rate between CO₂ and the PZ. Curiously, the experimental CO₂ flux is lower at 331 K than at 319 K. This is related to the decrease of the input CO₂ molar fractions at 333 K due to the higher water content within the gas phase at these conditions. The CO₂ solubility decreases as temperature increases, which can also explain the observed evolution of fluxes.

The analysis of the simulated PZ concentration profiles in the liquid film at the reactor outlet (Fig. 10) shows that the PZ depletion at the gas-liquid interface remains moderate in all conditions. The CO₂ mass transfer is thus mainly governed by the CO₂ diffusion and the kinetics of the system.

4.2.2 Loaded Solutions

Experiments were performed in order to study the reaction between PZCOO⁻ and CO₂. The experimental tests were carried out at 298 and 331 K in 1 M PZ solutions and for initial loadings of 0.2, 0.3 and 0.4 mol_{CO₂}/mol_{PZ}. The loadings led to high PZCOO⁻ concentrations without too much modifying the physicochemical properties of the liquid solution.

Experimental results and corresponding simulations are reported in Table 5. As for unloaded solutions, the simulations were performed considering the experimental temperature and input CO₂ molar fraction. Again, model predictions were in very good agreement with simulations, the AAD between model and experimental data being 2.7%.

The influence of the second amine-function on the CO₂ flux has been quantified by performing simulations neglecting the dicarbamate formation, the results being reported in the last column of Table 5. In this case, the model systematically underestimated the CO₂ flux, the average difference between model and experiments being of about 10%. Consequently, the dicarbamate formation has to be taken into account to predict the CO₂ global transfer at these conditions.

The variation of the absorption flux with the solution loading is shown in Figure 11 for the two investigated temperatures. Measurements and simulations are shown, the simulations being performed at the average temperature and CO₂ inlet molar fraction of the measurement series.

At a given temperature, the absorption flux decreases with the solution loading. This can be explained by the fact that the concentration of PZ + PZCOO⁻ decreases with solution loading whereas the CO₂ equilibrium vapour pressure increases. As a result, both the reaction rates and the driving force decrease, leading to a reduction of the CO₂ flux.

TABLE 4
Experimental results of CO₂ absorption into unloaded PZ solutions

Total [PZ]	Temperature	Gas mass transfer resistance	CO ₂ gas phase composition		CO ₂ flux ($\times 10^3$)	
			Inlet	Outlet	Experimental	Simulated
M	K	%	ppmvol	ppmvol	mol.m ⁻² .s ⁻¹	mol.m ⁻² .s ⁻¹
0.2	296.6	18	7 085	5 130	1.05	1.07
0.6	297.0	29	7 008	4 147	1.55	1.47
1.0	297.3	37	6 870	3 583	1.82	1.62
0.2	318.8	22	7 211	4 580	1.30	1.20
0.6	319.0	30	7 331	3 890	1.67	1.63
1.0	318.8	35	7 300	3 554	1.83	1.79
0.2	331.4	20	6 905	4 240	1.13	1.16
0.6	331.0	30	6 799	3 306	1.50	1.50
1.0	330.9	35	6 864	2 987	1.65	1.65

$Q_L = 16$ L/h, $Q_G = 150$ NL/h, $P = 1.5$ bar.

TABLE 5
Experimental results of CO₂ absorption into loaded 1 M PZ solutions

Loading	Temperature	Gas mass transfer resistance	CO ₂ gas phase composition		CO ₂ flux ($\times 10^3$)		
			Inlet	Outlet	Experimental	Simulated	Simulated neglecting dicarbamate formation (Eq. 18)
mol _{CO₂} /mol _{PZ}	K	%	ppmvol	ppmvol	mol.m ⁻² .s ⁻¹	mol.m ⁻² .s ⁻¹	mol.m ⁻² .s ⁻¹
0.2	297.8	29	7 280	4 214	1.60	1.57	1.47
0.3	297.0	27	7 002	4 309	1.46	1.44	1.27
0.4	294.7	24	7 310	4 679	1.37	1.38	1.14
0.4	328.1	26	7 005	4 369	1.10	1.11	0.97
0.3	330.3	28	7 005	3 865	1.31	1.36	1.26
0.2	329.8	32	6 843	3 275	1.52	1.50	1.43
0.4	330.5	27	6 921	4 440	1.05	1.04	0.91
0.4	300.0	27	7 135	4 412	1.47	1.39	1.15
0.3	297.7	27	7 103	4 370	1.48	1.46	1.30

$Q_L = 16$ L/h, $Q_G = 150$ NL/h, $P = 1.5$ bar.

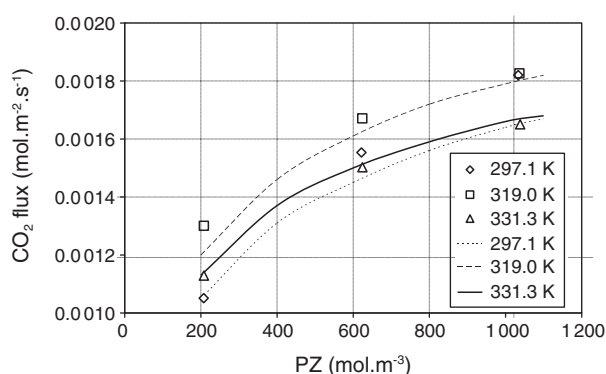


Figure 9

Variation of the absorption flux with total PZ concentration at 297, 319 and 331 K. Symbols: experiments; lines: simulations (at the average temperature and CO₂ inlet molar fraction of the experiments).

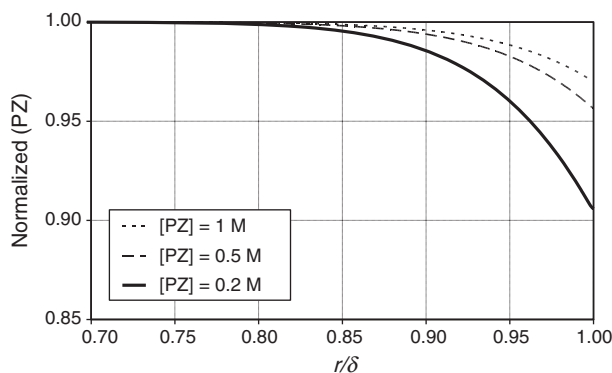


Figure 10

Simulated normalized PZ concentration profiles at the reactor outlet at 331 K.

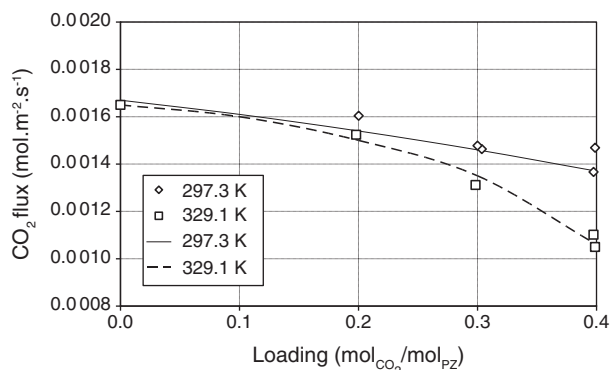


Figure 11

Variation of the absorption flux with solution loading at 297 and 329 K. Symbols: experiments; lines: simulations (at the average temperature and CO₂ inlet molar fraction of the experiments).

At a given loading, the absorption flux decreases with increasing operating temperature, the impact being more important at high solution loadings. The effective PZ + PZCOO⁻ concentration remains almost constant at iso-loading for the two investigated temperatures, but the increase of the CO₂ equilibrium vapour pressure is much more important at 329 K when compared to 298 K. As a result, the mass-transfer driving force decreases with temperature, leading to a decrease of the overall absorption flux.

CONCLUSION AND OUTLOOK

The paper describes theoretical and experimental investigations on the reactive absorption of CO₂ in aqueous solutions of PZ. A rigorous two dimensional absorption model, accounting for kinetics, hydrodynamics and thermodynamics, has been developed for a wetted wall column. The model considers the variation of the CO₂ gas phase concentration over the reactor length, which is more rigorous than previously published work, where average concentrations are considered. Model simulations clearly showed that the gas-phase concentration variation has to be taken into account, especially to assess the kinetics of CO₂ absorption in loaded solutions. The gas-liquid equilibrium was computed using the e-NRTL model, ensuring thus consistency of equations at the gas-liquid interface. The validity of equilibrium calculations has been shown by comparison between model simulations and gas-liquid equilibrium measurement taken from literature.

Model simulations allowed to define accurate operating conditions, where the diffusion of the liquid-side reactants were hardly limiting. However some free PZ depletion was always observed at the gas-liquid interface.

A laboratory-scale wetted wall column was conceived and constructed and the gas-side mass-transfer coefficient was determined experimentally. CO₂ absorption experiments were carried out at different temperatures in the experimental device in loaded as well as in unloaded PZ solutions. The gas-side mass transfer resistance was shown to be responsible of about 30% of the overall mass transfer resistance. Thus the knowledge of the gas-side mass transfer coefficient is crucial in order to correctly interpret absorption measurements.

When applying the kinetic constants published by [Bishnoi and Rochelle \(2002\)](#) the reactor model permits to predict the absorption fluxes with a global AAD of only 3.2% between theory and experiments. It has been shown that in loaded solutions the dicarbamate formation has to be taken into account in order to accurately

predict the absorption flux. The model and the experimental device will be used in the future in order to investigate the absorption kinetics in more complex, mixed amine solutions.

REFERENCES

- Appl M., Wagner U., Henrici H.J., Kuessner K., Volkamer F., Ernst-Neust N. (1982) Removal of CO₂ and/or H₂S and/or COS from gases containing these constituents, *US Patent* 4336233.
- Bindwal A.B., Vaidya P.D., Kenig E.Y. (2011) Kinetics of carbon dioxide removal by aqueous diamines, *Chem. Eng. J.* **169**, 1-3, 144-150.
- Bishnoi S. (2000) Carbon Dioxide Absorption and Solution Equilibrium in Piperazine Activated Methyldiethanolamine, *PhD Dissertation*, The University of Texas.
- Bishnoi S., Rochelle G.T. (2000) Absorption of carbon dioxide into aqueous piperazine: reactions kinetics, mass transfer and solubility, *Chem. Eng. Sci.* **55**, 22, 5531-5543.
- Bishnoi S., Rochelle G.T. (2002) Absorption of carbon dioxide in aqueous piperazine/methyldiethanolamine, *AIChE J.* **48**, 2788-2799.
- Caplow M. (1968) Kinetics of carbamate formation and breakdown, *J. Am. Chem. Soc.* **90**, 6795-6803.
- Chakravarty T., Phukan U.K., Weiland R.H. (1985) Reaction of Acid Gases with Mixtures of Amines, *Chem. Eng. Prog.* **81**, 32-36.
- Crooks J.E., Donnellan J.P. (1989) Kinetics and Mechanism of the Reaction Between Carbon-Dioxide and Amines in Aqueous-Solution, *J. Chem. Soc.-Perkin Transa.* **2**, 331-333.
- Cullinane J.T. (2005) Thermodynamics and Kinetics of Aqueous Piperazine with Potassium Carbonate for Carbon Dioxide Absorption, *PhD Dissertation*, The University of Texas.
- Danckwerts P.V. (1979) The reaction of CO₂ with ethanolamines, *Chem. Eng. Sci.* **34**, 443-446.
- da Silva E.F., Svendsen H.F. (2004) *Ab initio* study of the reaction of carbamate formation from CO₂ and alkanolamines, *Ind. Eng. Chem. Res.* **43**, 3413-3418.
- DeCoursey W. (1974) Absorption with chemical reaction: development of a new relation for the Danckwerts model, *Chem. Eng. Sci.* **29**, 1867-1872.
- Derks P.W.J., Kleingeld T., van Aken C., Hogendoorn J.A., Versteeg G.F. (2006) Kinetics of absorption of carbon dioxide in aqueous piperazine solutions, *Chem. Eng. Sci.* **61**, 6837-6854.
- Dugas R. (2009) Carbon Dioxide Absorption, Desorption, and Diffusion in Aqueous Piperazine and Monoethanolamine, *PhD Dissertation*, The University of Texas.
- Hamborg E.S., Versteeg G.F. (2009) Dissociation Constants and Thermodynamic Properties of Amines and Alkanolamines from (293 to 353) K, *J. Chem. Eng. Data* **54**, 1318-1328.
- Hilliard M. (2005) Thermodynamics of Aqueous Piperazine/Potassium Carbonate/Carbon Dioxide Characterized by the Electrolyte NRT Model within Aspen Plus®, *MS Thesis*, The University of Texas.
- Hogendoorn J., Vas Bhat R., Kuipers J., Van Swaaij W., Versteeg G. (1997) Approximation for the enhancement factor applicable to reversible reactions of finite rate in chemically loaded solutions, *Chem. Eng. Sci.* **52**, 4547-4559.
- Ko J.J., Tsai T.C., Lin C.Y. (2001) Diffusivity of nitrous oxide in aqueous alkanolamine solutions, *J. Chem. Eng. Data* **46**, 160-165.
- Littel R.J., Versteeg G.F., van Swaaij W.P.M. (1992) Kinetics of CO₂ with Primary and Secondary-Amines in Aqueous-Solutions. I. Zwitterion Deprotonation Kinetics for DEA and DIPA in Aqueous Blends of Alkanolamines, *Chem. Eng. Sci.* **47**, 2027-2035.
- Pacheco M. (1998) Mass Transfer, Kinetics and Rate-Based Modeling of Reactive Absorption, *PhD Dissertation*, The University of Texas.
- Pinsent B.R.W., Pearson L., Roughton F.J.W. (1956) The kinetics of combination of carbon dioxide with hydroxide ions, *Trans. Faraday Soc.* **52**, 1512-1520.
- Poling B.R., Prausnitz J.M., O'Connell J.P. (2000) *The Properties of gases and liquids*, McGraw-Hill, Fifth Edition.
- Rinker E.B., Ashour S.S., Sandall O.C. (1996) Kinetics and modeling of carbon dioxide absorption into aqueous solutions of diethanolamine, *Ind. Eng. Chem. Res.* **35**, 1107-1114.
- Rinker E.B., Ashoun S.S., Sandall O.C. (2000) Absorption of carbon dioxide into aqueous blends of diethanolamine and methyldiethanolamine, *Ind. Eng. Chem. Res.* **39**, 4346-4356.
- Samanta A., Roy S., Bandyopadhyay S.S. (2007) Physical Solubility and Diffusivity of N₂O and CO₂ in Aqueous Solutions of Piperazine and (N-Methyldiethanolamine + Piperazine), *J. Chem. Eng. Data* **52**, 1381-1385.
- Samanta A., Bandyopadhyay S.S. (2007) Kinetics and modeling of carbon dioxide absorption into aqueous solutions of piperazine, *Chem. Eng. Sci.* **62**, 7312-7319.
- Seo D.J., Hong W.H. (2000) Effect of piperazine on the kinetics of carbon dioxide with aqueous solutions of 2-amino-2-methyl-1-propanol, *Ind. Eng. Chem. Res.* **39**, 2062-2067.
- Versteeg G.F., Van Dijck L.A.J., Van Swaaij W.P.M. (1996) On the kinetics between CO₂ and alkanolamines both in aqueous and non-aqueous solutions, An overview. *Chemical Engineering Communications* **144**, 113-158.
- Xu G.W., Zhang C., Qin S., Wang Y. (1992) Kinetics Study on Absorption of Carbon-Dioxide Into Solutions of Activated Methyldiethanolamine, *Ind. Eng. Chem. Res.* **31**, 921-927.

Manuscript accepted in April 2013

Published online in January 2014

Copyright © 2014 IFP Energies nouvelles

Permission to make digital or hard copies of part or all of this work for personal or classroom use is granted without fee provided that copies are not made or distributed for profit or commercial advantage and that copies bear this notice and the full citation on the first page. Copyrights for components of this work owned by others than IFP Energies nouvelles must be honored. Abstracting with credit is permitted. To copy otherwise, to republish, to post on servers, or to redistribute to lists, requires prior specific permission and/or a fee: Request permission from Information Mission, IFP Energies nouvelles, fax. +33 1 47 52 70 96, or revueogst@ifpen.fr.

APPENDIX A

The gas phase material balance, assuming a plug-flow behaviour can be expressed as follows:

$$v_G \frac{\partial C_{\text{CO}_2}}{\partial z} = k_G a (C_{\text{CO}_2} RT - P^*) \quad (\text{A.1})$$

The integration of Equation (A.1), considering a constant equilibrium partial pressure at the gas-liquid interface gives:

$$\ln \frac{C_{\text{CO}_2}^{\text{out}} - C^*}{C_{\text{CO}_2}^{\text{in}} - C^*} = \frac{k_G a}{RT v_G} h \quad (\text{A.2})$$

If a CSTR model is used to perform the gas phase material balance:

$$Q_v^{\text{Gas}} (C_{\text{CO}_2}^{\text{outlet}} - C_{\text{CO}_2}^{\text{inlet}}) = \frac{k_G A}{RT} \times B \quad (\text{A.3})$$

Equations (A.2) and (A.3) are identical if B is given by:

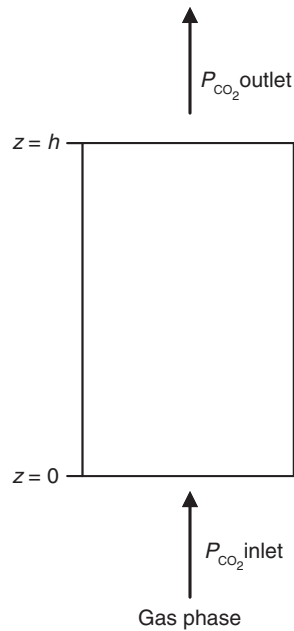


Figure A.1
Representation of the gas phase.

$$B = \frac{C_{\text{CO}_2}^{\text{out}} - C_{\text{CO}_2}^{\text{in}}}{\ln \frac{C_{\text{CO}_2}^{\text{out}} - C^*}{C_{\text{CO}_2}^{\text{in}} - C^*}} \quad (\text{A.4})$$

Consequently, both approaches gives identical results if C^* is constant within the reactor.

APPENDIX B

The mass transfer coefficient in the gas phase, k_G , was determined using CO_2 absorption measurements on MEA solutions at different concentrations. The gas flow was set to 150 L/h for all the experiments. A plug flow model was considered to characterize the gas phase flow, and the double film theory was used to model the mass transfer between the gas and the liquid phase. The CO_2 material balance within the gas phase was then given by:

$$F_{\text{CO}_2}|_z - F_{\text{CO}_2}|_{z+dz} = \frac{A}{\frac{1}{k_G} + \frac{H}{Ek_L}} P_{\text{CO}_2} \quad (\text{B.1})$$

After integration, the following expression is obtained:

$$\ln \frac{y_{\text{CO}_2}^{\text{out}}}{1 - y_{\text{CO}_2}^{\text{out}}} + \frac{y_{\text{CO}_2}^{\text{out}}}{1 - y_{\text{CO}_2}^{\text{out}}} - \left(\ln \frac{y_{\text{CO}_2}^{\text{in}}}{1 - y_{\text{CO}_2}^{\text{in}}} + \frac{y_{\text{CO}_2}^{\text{in}}}{1 - y_{\text{CO}_2}^{\text{in}}} \right) = - \frac{\frac{AP}{F_{\text{inert}}}}{\frac{1}{k_G} + \frac{H}{Ek_L}} \quad (\text{B.2})$$

Assuming that the experimental tests are carried out in the kinetic regime, the CO_2 mass transfer is not limited by the MEA diffusion towards the gas-liquid interface. Considering that the perfect gas law can be applied, the following equation is obtained. The hypothesis concerning the kinetic regime was verified afterwards:

$$\underbrace{\ln \frac{y_{\text{CO}_2}^{\text{out}}}{1 - y_{\text{CO}_2}^{\text{out}}} + \frac{y_{\text{CO}_2}^{\text{out}}}{1 - y_{\text{CO}_2}^{\text{out}}}}_y - \underbrace{\left(\ln \frac{y_{\text{CO}_2}^{\text{in}}}{1 - y_{\text{CO}_2}^{\text{in}}} + \frac{y_{\text{CO}_2}^{\text{in}}}{1 - y_{\text{CO}_2}^{\text{in}}} \right)}_x = - \frac{\frac{ART}{Q_{\text{inert}}}}{\frac{1}{k_G} + \frac{H}{\sqrt{D_{\text{CO}_2} k_{[\text{MEA}]}}}} \quad (\text{B.3})$$

After rearrangement:

$$\frac{1}{\underbrace{\ln \frac{y_{\text{CO}_2}^{\text{out}}}{1 - y_{\text{CO}_2}^{\text{out}}} + \frac{y_{\text{CO}_2}^{\text{out}}}{1 - y_{\text{CO}_2}^{\text{out}}}}_y} = \frac{Q_{\text{inert}}}{ARTk_G} + \frac{HQ_{\text{inert}}}{ART\sqrt{D_{\text{CO}_2}k}} \frac{1}{\underbrace{\sqrt{[\text{MEA}]}}_x} \quad (\text{B.4})$$

A linear regression allows to simultaneously determine the value of the volumetric mass transfer conductance (k_G) and the gas-liquid mass transfer area (A).

The CO_2 solubility in aqueous solutions of MEA was calculated by the correlation provided by Pacheco (1998). The second-order kinetic constant was given by Versteeg *et al.* (1996) while the CO_2 diffusion coefficient in aqueous solutions of MEA was determined through the N_2O analogy (Ko *et al.*, 2001).